MPI-PhE/2000-19
Revised version
1 June 2001

A Measurement of the QCD Colour Factors using Event Shape Distributions at $\sqrt{s} = 14$ to 189 GeV

S. Kluth, P. A. Movilla Fernández, S. Bethke, C. Pahl and P. Pfeifenschneider

Max-Planck-Institut für Physik,
Werner-Heisenberg-Institut
Föhringer Ring 6
80805 Munich, Germany

Abstract

Measurements of the QCD colour factors C_A and C_F and of the number of active quark flavours n_f in the process $e^+e^- \to$ hadrons at high energy are presented. They are based on fits of $\mathcal{O}(\alpha_s^2)$+NLLA QCD calculations to distributions of the event shape observables $1-T$, C, B_T and B_W measured at centre-of-mass energies from 14 GeV to 189 GeV. Hadronisation effects are approximated with power correction calculations which also depend on the QCD gauge structure. In this approach potential biases from hadronisation models are reduced. Our results for individually measured quantities obtained from $1-T$ and C are

$$n_f = 5.64 \pm 1.35, \quad C_A = 2.88 \pm 0.27 \quad \text{and} \quad C_F = 1.45 \pm 0.27$$

in good agreement with QCD based on the SU(3) symmetry group where $n_f = 5$ for the energies considered here, $C_A = 3$ and $C_F = 4/3$. From simultaneous fits of C_A and C_F with $1-T$ and C we find

$$C_A = 2.84 \pm 0.24 \quad \text{and} \quad C_F = 1.29 \pm 0.18\,,$$

which is also in good agreement with the QCD expectation.

(Submitted to European Physical Journal C)

1 Introduction

The theory of strong interactions, Quantum Chromo Dynamics (QCD), gives a successful description of most aspects of hadronic final states in e^+e^- annihilation and other high energy particle collision processes over a large range of centre-of-mass (cms) energies, see e.g. [1–10]. In particular, the strong coupling α_s, the only free parameter in the theory, can be measured to an accuracy of about 3% [11].

Standard QCD contains three distinct colour charges which are carried by the quarks and obey the SU(3) symmetry group, see e.g. [12, 13]. Requiring local gauge invariance of the theory generates eight massless vector fields, the gluons, each carrying a colour charge and an anticolour charge. Since the gluons are colour charged QCD has more fundamental vertices than QED, where the gauge boson, the photon, is electrically neutral. The fundamental vertices are i) the radiation of a gluon from a quark line (gluon bremsstrahlung), ii) the conversion of a gluon into a quark-antiquark pair (quark pair production), iii) the conversion of a gluon into two gluons (triple gluon vertex) and iv) the conversion of a gluon into three gluons (quartic gluon vertex). The quartic gluon vertex is in e^+e^- annihilation of order $\mathcal{O}(\alpha_s^3)$ and thus inaccessible to the $\mathcal{O}(\alpha_s^2)$ analysis presented here (see section 2).

The relative weights of each of the vertices are given by the QCD colour factors C_F, T_F and C_A corresponding to vertices i), ii) and iii), respectively [12]. The colour factor T_F for vertex ii) contributes for each of n_f active quark flavours, such that the product $T_F n_f$ is the weight for vertex ii).

The colour factors can be calculated from the generators of gauge transformations in the fundamental and adjoint representation once a particular symmetry group has been chosen. In standard QCD the symmetry group is SU(3) and the corresponding values of the colour factors are $C_F = 4/3$, $T_F = 1/2$ and $C_A = 3$. Perturbative QCD calculations, e.g. for cross sections, depend on the symmetry group only through the colour factors. It is thus straightforward to modify the prediction for a different symmetry group by recalculating the colour factors.

From an experimental point of view one can ask the question if SU(3) is indeed the correct symmetry group for QCD. This question may be tested experimentally by allowing the colour factors to vary in comparisons of QCD predictions with data. Several such studies have been performed by the LEP experiments based on correlations of angles in 4-jet final states [14–20]. In these studies the colour factors enter at leading order ($\mathcal{O}(\alpha_s^2)$) of the QCD calculations and thus higher order corrections have not been taken into account. Measurements of the ratios n_f/C_F and C_A/C_F by this method have been in agreement with the QCD expectations.

A complementary approach has been to employ distributions of event shape observables measured at LEP 1 and $\mathcal{O}(\alpha_s^2)$+NLLA[1] QCD predictions [21, 22]. Here the sensitivity to the colour factors also enters at $\mathcal{O}(\alpha_s^2)$ but higher order corrections are partially taken care of by the inclusion of the NLLA terms. More recent works combined the two analysis techniques outlined above [23] and also made use of recently calculated higher order corrections to the 4-jet angular correlations [24]. In both cases results have been

[1] NLLA stands for Next-to-Leading-Log Approximation, see section 2.

consistent with QCD predictions and systematic uncertainties were reduced[2].

It is also possible to use the dependence of QCD predictions on the energy scale of the hard process to gain sensitivity to the colour factors [11, 26, 27]. The dependence of QCD predictions on the energy scale enters through the running of the strong coupling α_s which in turn is a function of the colour factors.

A common property of all studies discussed so far is that they rely on Monte Carlo models of the hadronisation process, typically JETSET [28], HERWIG [29] or ARIADNE [30]. Dependence on these hadronisation models in studies of the QCD gauge structure may be viewed as a disadvantage, because the models assume standard QCD with the SU(3) symmetry group to be valid. No attempt was made to study the effects of non-standard colour factors on the hadronisation corrections. However, such effects could be significant, because the parton shower stages in the Monte Carlo models are based on QCD calculations which in turn depend on the QCD gauge symmetry.

Recently an analytic model of the hadronisation process has become available [31] commonly referred to as power corrections. It is based on the analysis of the power-behaviour of non-perturbative effects, i.e. the growth of non-perturbative effects with inverse powers of the scale of the hard process. In this model approximate predictions for the non-perturbative effects on mean values and distributions of some event shape observables have been made and their colour structure is explicitly given [32–37]. Comparison with data has been reasonably successful [5, 6, 27, 38–40].

In this study we use fits of $\mathcal{O}(\alpha_s^2)$+NLLA QCD predictions with power corrections to differential distributions of the event shape observables Thrust, C-parameter, Total and Wide Jet Broadening measured in e^+e^- annihilation at cms energies from 14 GeV to 189 GeV to investigate the gauge structure of QCD. Section 2 introduces the observables and summarises the QCD predictions. Section 3 gives a description of the data sets used in the analysis and of the fit results. Finally in section 4 a summary and conclusions are given.

2 QCD Predictions

2.1 Event Shape Observables

We use the following event shape observables:

Thrust T This observable is defined by the expression [41, 42]

$$T = \max_{\vec{n}} \left(\frac{\sum_i |\vec{p}_i \cdot \vec{n}|}{\sum_i |\vec{p}_i|} \right) \tag{1}$$

where p_i is the momentum of reconstructed particle i in an event. The thrust axis $\vec{n}_T$ is the direction $\vec{n}$ for which the maximum occurs. We will use the form $1-T$ here since its distribution is in this form more similar to those of the other observables.

[2]The error treatment of the results of [23] have been criticised [25].

C-parameter C The definition of this observable [43, 44] requires the introduction of the linearised energy-momentum tensor

$$\Theta^{\alpha\beta} = \frac{\sum_i (p_i^\alpha p_i^\beta)/|\vec{p}_i|}{\sum_i |\vec{p}_i|} \quad , \quad \alpha, \beta = 1, 2, 3 \tag{2}$$

and its three eigenvalues λ_k, $k = 1, 2, 3$. These define C via

$$C = 3(\lambda_1\lambda_2 + \lambda_2\lambda_3 + \lambda_3\lambda_1) \quad . \tag{3}$$

Note that C may equivalently be calculated by $C = (3/\sum_i |p_i|) \sum_{i<j} |\vec{p}_i||\vec{p}_j| \sin^2(\theta_{ij})$ where θ_{ij} is the angle between particles i and j.

Jet Broadening The definitions of the jet broadening observables [45] employ a plane through the origin perpendicular to the thrust axis $\vec{n}_T$ to divide the event into two hemispheres S_1 and S_2. The Total and the Wide Jet Broadening B_T and B_W are defined as

$$B_i = \frac{\sum_{p \in S_i} |\vec{p} \times \vec{n}_T|}{2 \sum_j |\vec{p}_j|} \quad , \quad B_T = B_1 + B_2 \quad , \quad B_W = \max(B_1, B_2) \quad . \tag{4}$$

For these observables complete $\mathcal{O}(\alpha_s^2)$+NLLA QCD predictions as well as power correction calculations for their differential distributions are available.

2.2 Running of α_s

The running of the strong coupling α_s is a direct consequence of the requirement that a complete QCD calculation, e.g. for a cross section R, should not depend on the choice of energy scale where the theory has been renormalised, formally expressed as the renormalisation group equation (RGE), see e.g. [13]:

$$\mu^2 \frac{dR}{d\mu^2} = \mu^2 \left(\frac{\partial}{\partial \mu^2} + \frac{\partial \alpha_s}{\partial \mu^2} \frac{\partial}{\partial \alpha_s} \right) R = 0 \quad . \tag{5}$$

The running of α_s is found by solving the following differential equation where $\beta(\alpha_s(\mu^2))$ is the beta function of QCD shown at two-loop accuracy [13]:

$$\mu^2 \frac{\partial \alpha_s}{\partial \mu^2} = \beta(\alpha_s(\mu)) = -\beta_0 \alpha_s^2(\mu) - \beta_1 \alpha_s^3(\mu) \quad , \tag{6}$$

$$\beta_0 = \frac{11C_A - 2n_f}{12\pi} \quad \text{and} \quad \beta_1 = \frac{17C_A^2 - 5C_A n_f - 3C_F n_f}{24\pi^2} \quad .$$

The coefficients β_0 and β_1 are independent of the renormalisation scheme. The solution to equation (6) at this order is [13, 22]

$$\beta_0 \ln(x_\mu^2) = \frac{1}{\alpha_s(\mu)} - \frac{1}{\alpha_s(Q)} + \frac{\beta_1}{\beta_0} \ln\left(\frac{\alpha_s(\mu)}{\alpha_s(Q)} \cdot \frac{\beta_0 + \beta_1 \alpha_s(Q)}{\beta_0 + \beta_1 \alpha_s(\mu)} \right) \tag{7}$$

with $x_\mu = \mu/Q$. The quantity x_μ is commonly referred to as the renormalisation scale factor since it allows to study the effects of variations of the renormalisation scale in perturbative QCD predictions. It is usually varied to assess the effect of missing higher order in the perturbation series. Equation (7) may be solved numerically to obtain $\alpha_s(\mu)$ as a function of a reference $\alpha_s(Q)$. The QCD gauge structure enters via the coefficients β_0 and β_1 of the QCD β-function.

The perturbative evolution of α_s diverges for small scales, see e.g. [13]. The location of the divergence, referred to as the Landau pole, defines the parameter $\Lambda_{\rm QCD}$ which in $\mathcal{O}(\alpha_s)$ is given implicitly by $\alpha_s(Q) = 1/(\beta_0 \ln(Q^2/\Lambda^2_{\rm QCD}))$. The value of $\Lambda_{\rm QCD}$ is approximately 200 MeV and indicates the scale where perturbative evolution of α_s breaks down.

2.3 Perturbative QCD Calculations

The perturbative QCD prediction in $\mathcal{O}(\alpha_s^2)$ for a normalised differential event shape distribution dR_{PT}/dy of a generic observable y measured at cms energy $\sqrt{s} = Q$ may be written as follows [21, 22]:

$$\frac{dR_{PT}}{dy} = \frac{1}{\sigma_{tot}}\frac{d\sigma}{dy} = \frac{dA}{dy} C_F \hat{\alpha}_s(\mu) + \left(\left(\pi\beta_0 \ln(x_\mu^2) - \frac{3}{4} C_F \right) 2 C_F \frac{dA}{dy} + \frac{dB}{dy} \right) \hat{\alpha}_s^2(\mu) \quad . \tag{8}$$

Here σ_{tot} is the cross section for the process $e^+e^- \to$ hadrons, dA/dy and dB/dy are the $\mathcal{O}(\alpha_s)$ and the $\mathcal{O}(\alpha_s^2)$ coefficients, respectively, and $\hat{\alpha}_s = \alpha_s/(2\pi)$. The coefficients dB/dy are in fact a sum of three terms each proportional to a colour factor:

$$\frac{dB}{dy} = C_F \left(\frac{dB_{C_F}}{dy} C_F + \frac{dB_{C_A}}{dy} C_A + \frac{dB_{n_f}}{dy} n_f \right) \quad . \tag{9}$$

The coefficients dA/dy and dB_i/dy, $i = C_F, C_A, n_f$, are obtained by integrating the $\mathcal{O}(\alpha_s^2)$ QCD matrix elements [46] in the $\overline{\rm MS}$ renormalisation scheme using the program EVENT2 [47]. A QCD prediction in $\mathcal{O}(\alpha_s^2)$ is expected to be valid in a region of phase space where the radiation of a single hard gluon dominates (3-jet region).

For the observables considered here calculations in NLLA have been performed [35, 48, 49]. The NLLA is valid in a region of phase space where multiple radiation of soft and collinear gluons from a system of two hard and back-to-back partons dominates (2-jet region). In the NLLA the cumulative normalised cross section $R_{NLLA}(y)$ is written as:

$$R_{NLLA}(y) = \int_0^y \frac{1}{\sigma_{tot}} \frac{d\sigma}{dy'} dy' = C(\alpha_s) e^{G(\alpha_s, L)} \tag{10}$$

with $L = \ln(1/y)$. The functions $C(\alpha_s)$ and $G(\alpha_s, L)$ are known in NLLA as:

$$C(\alpha_s) = 1 + C_1 \hat{\alpha}_s + C_2 \hat{\alpha}_s^2 \quad \text{and} \quad G(\alpha_s, L) = \sum_{n=1}^{\infty} \sum_{m=1}^{n+1} G_{nm} \hat{\alpha}_s^n L^m \simeq L g_1(L\alpha_s) + g_2(L\alpha_s) \quad . \tag{11}$$

The coefficients C_1, G_{11}, G_{12}, G_{22} and G_{23} are known analytically with complete colour structure while analytical expressions for the coefficients C_2 and G_{21} are not available.

The combination of the $\mathcal{O}(\alpha_s^2)$ and the NLLA calculations is a procedure called matching. Several matching schemes have been used in measurements of α_s, see e.g. [50]. We choose to employ the so-called $\ln(R)$-matching scheme with the following implementation [50]:

$$\begin{aligned} \ln R_{PT}(y) &= Lg_1(L\alpha_s) + g_2(L\alpha_s) - (G_{11}L + G_{12}L^2)\hat{\alpha}_s - (G_{22}L^2 + G_{23}L^3)\hat{\alpha}_s^2 \\ &\quad + A(y)\hat{\alpha}_s + (B(y) - \frac{1}{2}A(y)^2)\hat{\alpha}_s^2 \quad . \end{aligned} \tag{12}$$

The subtraction of the G_{nm} coefficients takes account of the contributions contained in the NLLA as well as in the $\mathcal{O}(\alpha_s^2)$ calculations. The term $A(y)$ is defined by $A(y) = \int_0^y (dA/dy')dy'$ and equivalently $B(y) = \int_0^y (dB/dy')dy'$. Our choice of the $\ln(R)$-matching scheme is motivated by two arguments, i) it is preferred theoretically [48] as well as experimentally [50] and ii) it depends only on G_{nm} coefficients known analytically with full colour structure.

2.4 Non-perturbative QCD Calculations: Power Corrections

The model of Dokshitzer, Marchesini and Webber (DMW) [31] treats the effects of gluon radiation at low energy scales ($\mathcal{O}(\Lambda_{\rm QCD})$) where simple perturbative evolution of α_s breaks down due to the presence of the Landau pole. The model assumes that evolution of the strong coupling α_s down to energies around and below the Landau pole is possible. The form of $\alpha_s(\mu)$ at such low energy scales is a priori unknown and a non-perturbative parameter is introduced as the 0th moment over $\alpha_s(\mu)$:

$$\alpha_0 = \frac{1}{\mu_I}\int_0^{\mu_I} \alpha_s(k)dk \quad . \tag{13}$$

The quantity μ_I is referred to as the infrared matching scale where the non-perturbative and standard perturbative evolution of α_s are merged, generally taken to be 2 GeV.

For the observables considered here the power corrections to the differential distributions have been calculated up to two loops [36, 51]. It turns out that a distribution dR/dy measured at cms energy $\sqrt{s} = Q$ can be described by the shifted perturbative prediction dR_{PT}/dy:

$$\frac{dR}{dy} = \frac{dR_{PT}}{dy}(y - PD_y) \quad . \tag{14}$$

The factor P is universal [51] and depends mainly on the non-perturbative parameter α_0, the infrared matching scale μ_I and the cms energy Q:

$$P = \frac{4C_F}{\pi^2}\mathcal{M}\frac{\mu_I}{Q}\left(\alpha_0(\mu_I) - \alpha_s(Q) - 2\beta_0\alpha_s^2(Q)\left(\ln\frac{Q}{\mu_I} + \frac{K}{\beta_0} + 1\right)\right) \tag{15}$$

with $K = (67/18 - \pi^2/6)C_A - (5/9)n_f$ for the $\overline{\rm MS}$ renormalisation scheme. The negative terms containing $\alpha_s(Q)$ are necessary for a consistent merging of the strong coupling in the non-perturbative and the perturbative region. The quantity $\mathcal{M}$ (Milan factor) stems from two-loop effects and is given by [37]

$$\mathcal{M} = 1 + (1.575C_A - 0.104n_f)/(4\pi\beta_0) \tag{16}$$

Its numerical value is 1.49 in standard QCD with $n_f = 3$ with an estimated theoretical uncertainty of 20% [51]. The factor D_y in equation (14) is observable specific and is given by:

$$\begin{aligned} D_{1-T} &= 2 \\ D_C &= 3\pi \\ D_{B_T,B_W} &= \frac{1}{2}\ln\frac{1}{y} + F_y(y,\alpha_s(yQ)) \quad . \end{aligned} \tag{17}$$

The functions F_y, $y = B_T, B_W$, with known colour structure, describe additional changes to the distributions referred to as squeeze [36, 52].

3 Analysis of the Data

3.1 Event Shape Data

We use all published data on distributions of our observables T, C, B_T and B_W which include experimental systematic uncertainties in their errors. The data available in the fits are listed in table 1 with references and the ranges which are considered in the fits. The fit ranges are determined by the following criteria:

Data with $\sqrt{s} \geq M_{Z^0}$ We choose to follow the approach of the OPAL collaboration [2–4,50] because we use the same $\mathcal{O}(\alpha_s^2)$+NLLA calculations with the $\ln(R)$-matching. The OPAL collaboration required the experimental and hadronisation corrections to be reasonably uniform and not strongly model dependent within the fit ranges. In addition, bins at the edges of fit ranges with large χ^2 contributions were removed. The fit ranges of distributions of the other experiments are adjusted to match the ones of OPAL as closely as possible.

Data with $\sqrt{s} < M_{Z^0}$ We use the studies of the recently reanalysed JADE data as a guideline [5,6]. However, we require in addition that i) the fit ranges should extend less far into the 2-jet region than those used in [50] and ii) the distance between the extreme 2-jet region and the fit ranges should increase with decreasing $\sqrt{s}$. These requirements reduce the sensitivity of the analysis to hadronisation corrections which are generally larger in the 2-jet region than in the 3-jet region. We also demand that no single bin at the edge of a fit range should have a large χ^2 contribution.

Within these ranges experimental corrections for limited acceptance and resolution as well as non-perturbative effects as estimated with Monte Carlo models are well under control.

3.2 Fit Procedure

The fits are based on equation (7) for the running of α_s, on equation (12) for the perturbative QCD prediction and on equation (14) for the power corrections. We vary the strong coupling $\alpha_s(M_{Z^0})$ with the mass of the Z^0 boson as a reference scale, one colour factor, i.e. n_f, C_A or C_F, and optionally the non-perturbative parameter α_0 in the fits.

We also investigate fits where $\alpha_s(M_{Z^0})$, the two colour factors C_A and C_F and optionally α_0 are free parameters. Fixed parameters are always set to the values as expected in standard QCD, i.e. $n_f = 5$, $C_A = 3$ and $C_F = 4/3$. To avoid unphysical results and to stabilise the fits the free parameters are bounded by $0.01 < \alpha_s(M_{Z^0}) < 0.3$, $0 < n_f < 20$, $0 < C_A < 10$, $0 < C_F < 10$ and $0 < \alpha_0 < 10$.

The fit procedure minimises a χ^2 constructed from the difference in bin i between the data value d_i and the theoretical prediction t_i divided by the total error σ_i:

$$\chi^2 = \sum_{i \in \text{fitranges}} \left(\frac{d_i - t_i}{\sigma_i} \right)^2 \quad . \tag{18}$$

Possible correlations between bins of a given distribution or between different distributions are neglected. With the exception of the OPAL data for $1-T$, B_T and B_W at $\sqrt{s} = M_{Z^0}$ the data are measured in bins which are wider than the typical experimental resolution in order to reduce bin-to-bin migrations. Many of the distributions used in this analysis were measured by the same experiments such that the presence of some correlation between distributions may be expected. There may also be correlations between the data points of any given distribution due to common systematic uncertainties. However, information about such correlations is not available in the references for the data (see table 1).

The errors on the fitted parameters are calculated in the fit procedure from the diagonal elements of the covariance matrix after the fit has converged ("fit error"). These errors contain the contributions from statistical fluctuations and systematic uncertainties quoted by the individual experiments.

We follow two alternatives to study the influence of non-perturbative effects on our fits. Firstly, we fix the non-perturbative parameter α_0 at a previously measured value and repeat the fits with α_0 varied by its total errors. Secondly, we allow α_0 to vary in the fit. The fixed value of α_0 is taken from [6], $\alpha_0 = 0.473^{+0.058}_{-0.041}$. However, some modifications had to be applied. The measurement of [6] used an erroneous value of the Milan factor, $\mathcal{M} = 1.794$ instead of 1.49, both for $n_f = 3$. From equation (15) we infer that it is sufficient to scale α_0 by the ratio of the two values for $\mathcal{M}$ as a correction. In our study we vary the colour factor n_f and it would therefore be inconsistent to use two different values of n_f, i.e. $n_f = 5$ in the perturbative part and $n_f = 3$ in the non-perturbative part of the QCD prediction for massless quarks. To find our standard value of α_0 we scale it by the ratio of values for the Milan factor determined with $n_f = 3$ and $n_f = 5$, respectively. Our final value is $\alpha_0 = 0.543 \pm 0.058$ with symmetrised errors.

3.3 Effects of $b\overline{b}$ events at low $\sqrt{s}$

The presence of events from the reaction $e^+e^- \to b\overline{b}$ at low cms energies $\sqrt{s}$ can distort the event shape distributions, because the effects of weak decays of heavy B-hadrons on the topology of hadronic events cannot anymore be neglected. An additional potential problem arises from comparing QCD calculations based on massless quarks with data containing massive quarks at $\sqrt{s}$ close to the production threshold.

At $\sqrt{s} \ll M_{Z^0}$ $b\overline{b}$ events constitute about 9% of the total event samples. Ideally one would correct the data experimentally by identifying $b\overline{b}$ events and removing them from

the sample. However, since we have only published event shape data without information on specific quark flavours we resort to a correction based on Monte Carlo simulations. We generate samples of 10^6 events at each $\sqrt{s}$ with the JETSET 7.4 program [28] with the parameter set given in [53]. For each event shape observable we build the ratio of distributions calculated with u, d, s and c quark events to those calculated with all events. This ratio is multiplied with the bin contents of the data to obtain corrected distributions. This procedure is applied to all data at $\sqrt{s} < M_{\mathrm{Z}^0}$. It was verified that the simulation provides an adequate description of the data at all values of $\sqrt{s} < M_{\mathrm{Z}^0}$.

Systematic effects due to uncertainties in the Monte Carlo parameters are expected to be small for the ratio except for those parameters which only affect the $\mathrm{b\overline{b}}$ events in the samples. The most important such parameter is the value of ϵ_b in the Peterson fragmentation function [54] which controls the fragmentation of b quarks in the simulation. Threshold effects at low $\sqrt{s}$ which depend on the value of the b-quark mass in the simulation are found to be negligible for the fit results.

3.4 Systematic Variations

As systematic variations we consider the following changes in the analysis:

Renormalisation scale The standard fits are carried out with the renormalisation scale parameter $x_\mu = 1$. The dependence on the renormalisation scale is investigated by repeating the fits with $x_\mu = 0.5$ and $x_\mu = 2.0$ [50]. Deviations of the fit results w.r.t. the standard fits are taken as asymmetric uncertainties.

Power corrections ($\boldsymbol{\alpha_0}$ fixed) The standard fits with fixed α_0 employ $\alpha_0 = 0.543$, as explained above. The fits are repeated with α_0 varied by its error, i.e. $\alpha_0 = 0.485$ and $\alpha_0 = 0.601$. Again, deviations of the fit results w.r.t. the standard fits are taken as asymmetric uncertainties.

Power corrections ($\boldsymbol{\alpha_0}$ free) The standard fits use the Milan factor as given by equation (16). The fits are repeated with the Milan factor scaled by a factor of 0.8 and 1.2, respectively, and deviations w.r.t. results of the standard fits are considered as asymmetric uncertainties. We also change the value of the infrared matching scale μ_I from its standard value of 2 GeV to 1 GeV and 3 GeV, respectively, and repeat the fits. Deviations w.r.t. the standard results are counted as asymmetric uncertainties, except for α_0 where changing μ_I corresponds to a redefinition of the non-perturbative parameter α_0.

Fragmentation of b quarks The standard analysis is carried out with corrected data at $\sqrt{s} < M_{\mathrm{Z}^0}$ based on the JETSET tuning of [53] as explained in section 3.3. The value of the JETSET parameter ϵ_b is varied around its central value $\epsilon_b = 0.0038 \pm 0.0010$ by adding or subtracting its error and the analysis including correction of the data at $\sqrt{s} < M_{\mathrm{Z}^0}$ is repeated. Deviations w.r.t. the standard results are considered as asymmetric uncertainties.

Experimental uncertainties We change the composition of the data sets for the fits in two ways, i) the data measured at $\sqrt{s} = M_{\mathrm{Z}^0}$ are removed and ii) only data measured

at $\sqrt{s} \geq M_{Z^0}$ are used. The larger of the two deviations w.r.t. the standard result observed with the data set i) or ii) is considered as the systematic uncertainty from variations in the input data.

The systematic uncertainties from the renormalisation scale, the power corrections with α_0 either fixed or free, the fragmentation of b quarks and from the input data are added in quadrature with the error from the fit to arrive at the total error.

3.5 Fit Results

The tables 2, 3 and 4 present the results of two-parameter fits to $\alpha_s(M_{Z^0})$ and n_f, C_A or C_F, respectively, with α_0 fixed. The results of three-parameter fits to $\alpha_s(M_{Z^0})$, C_A and C_F are given in table 5. The results of three-parameter fits to $\alpha_s(M_{Z^0})$, α_0 and one of the colour factors n_f, C_A or C_F are shown in tables 6, 7 and 8, respectively, while table 9 displays the results of four-parameter fits to $\alpha_s(M_{Z^0})$, α_0, C_A and C_F. The rows labelled "hadr." contain the quadratic sum of the uncertainties from the power corrections and the fragmentation of b-quarks. The power correction uncertainties are the dominating contribution in all cases. The tables show symmetrised errors except for the fit to $\alpha_s(M_{Z^0})$ and n_f where the variation of α_0 leads to a large difference between the positive and negative error. Figures 1, 2 and 3 give a graphic display of the results.

We observe stable fits in all cases for the observables $1-T$ and C. The fit results from these observables for the colour factors are generally in good agreement with the expectations from standard QCD within their total uncertainties. The results for $\alpha_s(M_{Z^0})$ and α_0 are also generally consistent with previous measurements within their total uncertainties [6,11]. The fit of n_f and $\alpha_s(M_{Z^0})$ with $1-T$ is consistent with an earlier analysis using similar data [26]. The fit of $\alpha_s(M_{Z^0})$, α_0, C_A and C_F with C converges but has such large fit errors that sensitivity to the colour factors is essentially lost; consequently we do not show the results.

With the other two observables, B_T and B_W, we also find generally consistent results with standard QCD and previous measurements. However, fits of B_T to $\alpha_s(M_{Z^0})$ and n_f and fits of of B_W to $\alpha_s(M_{Z^0})$, C_A and C_F as well as to $\alpha_s(M_{Z^0})$ and single colour factors with α_0 free are unstable and we do not show these results. Our interpretation is that the QCD calculations with power corrections for $1-T$ and C provide an adequate description of the data while there are still effects in the data for B_T and B_W which are not well described by the $\mathcal{O}(\alpha_s^2)$+NLLA QCD calculations with power corrections [5,6,40,50].

The values of χ^2/d.o.f. are smaller than one in all cases, except the fit of $\alpha_s(M_{Z^0})$ and C_A with B_T where $\chi^2/\text{d.o.f.} = 1.01$. The small values of χ^2/d.o.f. are consistent with the good description of the data by the fitted predictions and probably indicate the presence of correlations between the data points used in a given fit.

We find that in all fits with α_0 free the variation of the Milan factor leads to significantly smaller systematic uncertainties than the variation of α_0 in fits with α_0 fixed. The fitted values of α_0 vary over ranges compatible with the total error of the fixed value of α_0 when the Milan factor is changed. This is consistent with [6] where the error on α_0 was dominated by the variation of the Milan factor. We conclude that the ratio of non-perturbative and perturbative contributions is well constrained by the data such that

changes in the Milan factor are compensated by similar changes with the opposite sign in α_0. As a consequence we find that the hadronisation systematic uncertainties of fits to the colour factors are reduced when α_0 is a free parameter while the fit errors increase due to the presence of an extra free parameter in the fit.

We observe that the experimental uncertainties estimated by repeating the fits with reduced data sets are larger in the fits with α_0 free. This effect is likely to be a reflection of the increased fit errors. We choose to keep the larger uncertainties since we cannot rule out the possibility that there are systematic effects in the data to which the fits with α_0 free are more sensitive than the fits with α_0 fixed.

In simultaneous fits with several free parameters correlations between them may influence the results. In table 10 we show the correlations observed in the standard fits with the observable $1-T$. In addition in the first row of table 10 the correlation observed in a fit with only $\alpha_s(M_{\mathrm{Z}^0})$ and α_0 as free parameters is displayed. The presence of large correlations in some fits causes increased fit errors and may also contribute to the experimental uncertainties. We find a similar pattern of correlations with the other observables C, B_T and B_W.

3.6 Combination of Results

We construct combined results only from fits to $1-T$ and C, because we found these to be stable in all cases. We choose to base the combination for individual colour factors on the fits with α_0 free since these results should be less biased by input values measured assuming standard QCD. They also have smaller hadronisation uncertainties as discussed above. We build unweighted averages of the fit results for the standard analysis and for all systematic variations. As the fit error we choose the smaller of the two individual fit errors and we then construct the total error in the same way as for an individual observable. In this way correlations between systematic variations of the observables are taken into account. We find as our final results for the individually measured colour factors:

$$\begin{aligned} n_f &= 5.64 \pm 0.79(\mathrm{fit}) \pm 0.32(\mathrm{scale}) \pm 0.48(\mathrm{had.}) \pm 0.93(\mathrm{exp.}) \\ &= 5.64 \pm 1.35, \\ C_A &= 2.88 \pm 0.16(\mathrm{fit}) \pm 0.06(\mathrm{scale}) \pm 0.10(\mathrm{had.}) \pm 0.18(\mathrm{exp.}) \\ &= 2.88 \pm 0.27 \quad \text{and} \\ C_F &= 1.45 \pm 0.21(\mathrm{fit}) \pm 0.04(\mathrm{scale}) \pm 0.04(\mathrm{had.}) \pm 0.16(\mathrm{exp.}) \\ &= 1.45 \pm 0.27. \end{aligned} \tag{19}$$

The total uncertainties for all three colour factors are dominated by the fit error and the experimental uncertainties. The results are in good agreement with the expectation from standard QCD with five active quark flavours. The results for $\alpha_s(M_{\mathrm{Z}^0})$ and α_0 from the combination are consistent with the individual fits and with previous measurements [6,11], see table 11.

In the case of n_f the combined result has a slightly larger total uncertainty than the individual result based on the observable $1-T$ shown in table 6. This is mainly due to

the increased experimental uncertainty of the combined result which in turn is dominated by the experimental uncertainty of the fit with C. For the other colour factors C_A and C_F the total uncertainties of the combined results are somewhat smaller than the total uncertainties of the individual results. These observations are consistent, since we do not expect the total uncertainties to be greatly reduced by a combination of individual results due to the large correlations between the event shape distributions.

A combined result for the results of the simultaneous fits of C_A and C_F may only be constructed from the fits with α_0 fixed, because in the fits with α_0 free we obtained usable fits only for the observable $1-T$. Applying the same procedure as outlined above yields the following results for combining the results of the fits with the observables $1-T$ and C shown in table 5:

$$\begin{aligned} C_A &= 2.84 \pm 0.13(\text{fit}) \pm 0.06(\text{scale}) \pm 0.11(\text{had.}) \pm 0.15(\text{exp.}) \\ &= 2.84 \pm 0.24 \quad \text{and} \\ C_F &= 1.29 \pm 0.07(\text{fit}) \pm 0.17(\text{had.}) \pm 0.02(\text{exp.}) \\ &= 1.29 \pm 0.18. \end{aligned} \tag{20}$$

The scale uncertainty of the combined result for C_F is smaller than 0.01 consistent with the small scale uncertainties of the individual results, see table 5. The results for C_A and C_F are in good agreement with the combined results discussed above, see equation (19). The combined result for $\alpha_s(M_{\mathrm{Z}^0})$ is in agreement with the individual results and also with [11], see table 11.

The averaged correlation coefficient from the fits is $\rho_{C_A-C_F} = -0.89$. However, we observe that variations of the results for C_A and C_F are positively correlated when α_0 is changed. In order to find a conservative estimate of the correlation coefficient we construct a covariance matrix by summing i) the covariance matrix from the fit and ii) one covariance matrix for each systematic uncertainty. The covariance matrices ii) are constructed from the systematic uncertainties, symmetrised if necessary, and $\rho_{C_A-C_F} = -0.89$, except for the systematic uncertainty from the variation of α_0 where $\rho_{C_A-C_F} = 1.0$ is used. The resulting total correlation coefficient is $\rho_{C_A-C_F} = 0.19$. Figure 4 presents the combined results which are in good agreement with standard QCD within the uncertainties. Some other possible gauge groups are indicated including $\mathrm{U}(1)^3$, an abelian QCD with three quark colours and colour neutral gluons. Our results exclude all shown alternatives to SU(3) as the gauge group of QCD at more than 95% confidence level.

4 Summary and Conclusions

We have studied fits of $\mathcal{O}(\alpha_s^2)$+NLLA QCD predictions for distributions of the event shape observables $1-T$, C, B_T and B_W with power correction calculations to model hadronisation effects to data measured at cms energies ranging from 14 GeV to 189 GeV. In these fits we varied simultaneously the strong coupling $\alpha_s(M_{\mathrm{Z}^0})$, one of the QCD colour factors C_A or C_F, or the the number active quarks n_f, and in some cases also α_0, the free parameter of the power correction calculations. We investigated in addition fits, where $\alpha_s(M_{\mathrm{Z}^0})$, C_A and C_F and optionally α_0 were varied.

We found stable fits in all cases with the observables $1-T$ and C while some fits with B_T and in particular B_W appear unreliable. We take this as an indication that the current $\mathcal{O}(\alpha_s^2)$+NLLA QCD calculations with power corrections for B_T and B_W describe the data not as well as the same calculations for $1-T$ and C.

We observed that the variation of the Milan factor $\mathcal{M}$ and the infrared matching scale μ_I in the fits with α_0 free gave rise to smaller systematic uncertainties than the systematic variation of α_0 in the fits with α_0 fixed. Our conclusion is that the relative contributions of the perturbative $\mathcal{O}(\alpha_s^2)$+NLLA QCD calculations and the power correction terms to the total predictions are quite well constrained by the data.

A combination of the individual results of the fits with $\alpha_s(M_{\mathrm{Z}^0})$, an individual colour factor and α_0 as free parameters with the observables $1-T$ and C yields our final results:

$$\begin{aligned} n_f &= 5.64 \pm 1.35, \\ C_A &= 2.88 \pm 0.27 \quad \text{and} \\ C_F &= 1.45 \pm 0.27. \end{aligned}$$

The combination of results from simultaneous fits of C_A, C_F and $\alpha_s(M_{\mathrm{Z}^0})$ for α_0 fixed with the observables $1-T$ and C gives

$$C_A = 2.84 \pm 0.24 \quad \text{and} \quad C_F = 1.29 \pm 0.18 \tag{21}$$

with total correlation coefficient $\rho_{C_A - C_F} = 0.19$. These results are in good agreement with the expectation from standard QCD based on the SU(3) symmetry group for $\mathrm{e^+e^-}$ annihilation data at high energies, i.e. $n_f = 5$ with $T_F = 1/2$, $C_A = 3$ and $C_F = 4/3$. There is also good agreement between the individual and the simultaneous measurements of C_A and C_F. All combined results for $\alpha_s(M_{\mathrm{Z}^0})$ and α_0 are in agreement with previous measurements. We found that the total uncertainties of the combined results are approximately of the same size as the total uncertainties of the individual results. This is consistent, because the event shape distributions are correlated with each other and the total uncertainties are dominated by the fit errors and experimental uncertainties.

We present our final conclusions from two points of view. Firstly, we assume that the power correction calculations are a good model of hadronisation effects in event shape distributions. In this case we have performed a complementary test of the gauge structure of QCD with competitive uncertainties on the measurements of the QCD colour factors compared to other analyses [19,20,23,24]. Secondly, under the assumption that QCD with SU(3) group symmetry is the correct theory of strong interactions, our analysis provides a successful consistency check of the power correction calculations.

References

[1] JADE and OPAL Coll., P. Pfeifenschneider et al.: Eur. Phys. J. C 17 (2000) 19–51

[2] OPAL Coll., G. Abbiendi et al.: Eur. Phys. J. C 16 (2000) 185–210

[3] OPAL Coll., K. Ackerstaff et al.: Z. Phys. C 75 (1997) 193–207

[4] OPAL Coll., G. Alexander et al.: Z. Phys. C 72 (1996) 191–206

[5] JADE Coll., P. A. Movilla Fernández, O. Biebel, S. Bethke, S. Kluth, P. Pfeifenschneider et al.: Eur. Phys. J. C 1 (1998) 461–478

[6] JADE Coll., O. Biebel, P. A. Movilla Fernández, S. Bethke et al.: Phys. Lett. B 459 (1999) 326

[7] H1 Coll., C. Adloff et al.: DESY-00-145, (2000), Sub. to Eur. Phys. J. C

[8] ZEUS Coll., M. Derrick et al.: Z. Phys. C 72 (1996) 399–424

[9] D0 Coll., B. Abbott et al.: Phys. Rev. Lett. 82 (1999) 2451–2456

[10] O. Biebel: Phys. Rep. 340 (2001) 165–289

[11] S. Bethke: J. Phys. G 26 (2000) R27

[12] T. Muta: Foundations of Quantum Chromo Dynamics. Vol. 5 of World Scientific Lecture Notes in Physics, World Scientific (1987)

[13] R.K. Ellis, W.J. Stirling and B.R. Webber: QCD and Collider Physics. Vol. 8 of Cambridge Monographs on Particle Physics, Nuclear Physics and Cosmology, Cambridge University Press (1996)

[14] L3 Coll., B. Adeva et al.: Phys. Lett. B 248 (1990) 227

[15] OPAL Coll., M. Z. Akrawy et al.: Z. Phys. C 49 (1991) 49–57

[16] DELPHI Coll., P. Abreu et al.: Phys. Lett. B 255 (1991) 466

[17] ALEPH Coll., D. Decamp et al.: Phys. Lett. B 284 (1992) 151

[18] DELPHI Coll., P. Abreu et al.: Z. Phys. C 59 (1993) 357

[19] OPAL Coll., R. Akers et al.: Z. Phys. C 65 (1995) 367–377

[20] DELPHI Coll., P. Abreu et al.: Phys. Lett. B 414 (1997) 401–418

[21] N. Magnoli, P. Nason and R. Rattazzi: Phys. Lett. B 252 (1990) 271–281

[22] OPAL Coll., R. Akers et al.: Z. Phys. C 68 (1995) 519–530

[23] ALEPH Coll., R. Barate et al.: Z. Phys. C 76 (1997) 1–14

[24] B. Dienes: forthcoming, Presented at 30th International Symposium on Multiparticle Dynamics, Tihany, Hungary, October 9 - 15, 2000

[25] G. R. Farrar: In: 11ème Rencontre de Physique de la Vallée d'Aoste: Results and Perspectives in Particle Physics, La Thuile, Italy, 2-8 Mar 1997, M. Greco (ed.), Frascati physics series 9, pages 779–792. INFN Frascati, 1997

[26] T. Hebbeker: Z. Phys. C 60 (1993) 63–70

[27] L3 Coll., M. Acciarri et al.: Phys. Lett. B 489 (2000) 65–80

[28] T. Sjöstrand: Comput. Phys. Commun. 82 (1994) 74

[29] G. Marchesini et al.: Comput. Phys. Commun. 67 (1992) 465–508

[30] L. Lönnblad: Comput. Phys. Commun. 71 (1992) 15–31

[31] Yu.L. Dokshitzer, G. Marchesini and B.R. Webber: Nucl. Phys. B 469 (1996) 93–142

[32] Yu. L. Dokshitzer and B. R. Webber: Phys. Lett. B 352 (1995) 451–455

[33] Yu. L. Dokshitzer and B. R. Webber: Phys. Lett. B 404 (1997) 321–327

[34] Yu. L. Dokshitzer, A. Lucenti, G. Marchesini and G. P. Salam: Nucl. Phys. B 511 (1998) 396–418

[35] S. Catani and B. R. Webber: Phys. Lett. B 427 (1998) 377–384

[36] Yu. L. Dokshitzer, G. Marchesini and G. P. Salam: Eur. Phys. J. direct C 3 (1999) 1–45

[37] Yu. L. Dokshitzer: hep-ph/9911299 (1999), Invited talk at 11th Rencontres de Blois: Frontiers of Matter, Chateau de Blois, France, 28 Jun - 3 Jul 1999

[38] DELPHI Coll., P. Abreu et al.: Phys. Lett. B 456 (1999) 322–340

[39] H1 Coll., C. Adloff et al.: Eur. Phys. J. C 14 (2000) 255–269

[40] P. A. Movilla Fernández, O. Biebel and S. Bethke: PITHA 99/21, hep-ex/9906033 (1999), Contributed to International Europhysics Conference on High-Energy Physics (EPS-HEP 99), Tampere, Finland, 15-21 July

[41] S. Brandt, Ch. Peyrou, R. Sosnowski and A. Wroblewski: Phys. Lett. 12 (1964) 57–61

[42] E. Fahri: Phys. Rev. Lett. 39 (1977) 1587–1588

[43] G. Parisi: Phys. Lett. B 74 (1978) 65

[44] J. F. Donoghue, F. E. Low and S.Y. Pi: Phys. Rev. D 20 (1979) 2759

[45] S. Catani, G. Turnock and B.R. Webber: Phys. Lett. B 295 (1992) 269

[46] R.K. Ellis, D.A. Ross and A.E. Terrano: Nucl. Phys. B 178 (1981) 421

[47] S. Catani and M.H. Seymour: Phys. Lett. B 378 (1996) 287–301

[48] S. Catani, L. Trentadue, G. Turnock and B.R. Webber: Nucl. Phys. B 407 (1993) 3

[49] Yu. L. Dokshitzer, A. Lucenti, G. Marchesini and G. P. Salam: JHEP 1 (1998) 11

[50] OPAL Coll., P. D. Acton et al.: Z. Phys. C 59 (1993) 1–19

[51] Yu. L. Dokshitzer, A. Lucenti, G. Marchesini and G. P. Salam: JHEP 5 (1998) 3

[52] P. A. Movilla Fernández: Nucl. Phys. Proc. Suppl. 74 (1999) 384–387

[53] OPAL Coll., G. Alexander et al.: Z. Phys. C 69 (1996) 543–560

[54] C. Peterson, D. Schlatter, I. Schmitt and P. Zerwas: Phys. Rev. D 27 (1983) 105

[55] ALEPH Coll., D. Busculic et al.: Z. Phys. C 73 (1997) 409–420

[56] ALEPH Coll., D. Buskulic et al.: Z. Phys. C 55 (1992) 209–234

[57] DELPHI Coll., P. Abreu et al.: Z. Phys. C 73 (1996) 11–60

[58] L3 Coll., B. Adeva et al.: Z. Phys. C 55 (1992) 39–62

[59] OPAL Coll., P. D. Acton et al.: Z. Phys. C 55 (1992) 1–24

[60] SLD Coll., K. Abe et al.: Phys. Rev. D 51 (1995) 962

[61] AMY Coll., Y.K. Li et al.: Phys. Rev. D 41 (1990) 2675–2688

[62] TASSO Coll., W. Braunschweig et al.: Z. Phys. C 47 (1990) 187–198

[63] HRS Coll., D. Bender et al.: Phys. Rev. D 31 (1985) 1

[64] MARK II Coll., A. Petersen et al.: Phys. Rev. D 37 (1988) 1

Tables

$\sqrt{s}$	Experiment	$1-T$	C	B_T	B_W
189	L3 [27]	0.05-0.30	0.15-0.60	0.08-0.26	0.045-0.195
	OPAL [2]	0.04-0.30	0.18-0.60	0.075-0.25	0.05-0.20
183	DELPHI [38]	0.04-0.28	0.16-0.64	0.07-0.24	0.05-0.20
	L3 [27]	0.05-0.30	0.15-0.60	0.08-0.26	0.045-0.195
	OPAL [2]	0.04-0.30	0.18-0.60	0.075-0.25	0.05-0.20
172	DELPHI [38]	0.04-0.24	0.16-0.64	0.08-0.27	0.04-0.17
	L3 [27]	0.05-0.30	0.15-0.60	0.08-0.26	0.045-0.195
	OPAL [2]	0.04-0.30	0.18-0.60	0.075-0.25	0.05-0.20
161	DELPHI [38]	0.04-0.24	0.16-0.64	0.08-0.27	0.04-0.17
	L3 [27]	0.05-0.30	0.15-0.60	0.08-0.26	0.045-0.195
	OPAL [3]	0.04-0.30	0.18-0.60	0.075-0.25	0.05-0.20
133	ALEPH [55]	0.04-0.30			
	DELPHI [38]	0.04-0.24	0.16-0.64	0.08-0.27	0.04-0.17
	L3 [27]	0.05-0.25	0.15-0.64	0.08-0.26	0.045-0.195
	OPAL [4]	0.04-0.30	0.18-0.60	0.075-0.25	0.05-0.20
91	ALEPH [56]	0.06-0.30	0.20-0.64		
	DELPHI [57]	0.06-0.30	0.20-0.64	0.09-0.24	0.07-0.17
	L3 [58]	0.065-0.29	0.22-0.64		
	OPAL [50, 59]	0.06-0.30	0.20-0.64	0.09-0.23	0.07-0.17
	SLD [60]	0.06-0.26	0.24-0.64	0.08-0.26	0.08-0.20
55	AMY [61]	0.10-0.30			
44	JADE [5, 6]	0.08-0.30	0.24-0.58	0.10-0.24	0.08-0.18
	TASSO [62]	0.08-0.28			
35	JADE [5, 6]	0.08-0.30	0.24-0.58	0.10-0.24	0.08-0.18
	TASSO [62]	0.08-0.28			
29	HRS [63]	0.10-0.30			
	MARKII [64]	0.10-0.30			
22	TASSO [62]	0.10-0.28			
14	TASSO [62]	0.12-0.28			

Table 1: The sources of the data and the fit ranges for the observables $1-T$, C, B_T and B_W are shown. The cms energy $\sqrt{s}$ at which the experiments analysed their data is given in GeV.

	$1-T$		C		B_W	
	n_f	$\alpha_s(M_{Z^0})$	n_f	$\alpha_s(M_{Z^0})$	n_f	$\alpha_s(M_{Z^0})$
fit result	7.32	0.124	5.82	0.114	2.06	0.093
fit error	± 0.49	± 0.002	± 0.52	± 0.002	± 1.04	± 0.003
χ^2/d.o.f.	130.8/236		104.0/155		109.0/121	
ren. scale	± 0.11	± 0.003	± 0.55	± 0.002	± 1.33	± 0.002
hadr.	$^{+0.56}_{-2.39}$	± 0.007	± 2.30	± 0.006	± 1.47	± 0.003
exp.	± 0.42	± 0.003	± 1.95	± 0.006	± 2.89	± 0.010
tot. error	$^{+0.86}_{-2.48}$	± 0.008	± 3.14	± 0.009	± 3.66	± 0.011

Table 2: Results are shown for fits with the observables $1-T$, C and B_W to $\alpha_s(M_{Z^0})$ and n_f.

	$1-T$		C		B_T		B_W	
	C_A	$\alpha_s(M_{Z^0})$	C_A	$\alpha_s(M_{Z^0})$	C_A	$\alpha_s(M_{Z^0})$	C_A	$\alpha_s(M_{Z^0})$
fit result	2.62	0.123	2.88	0.113	3.82	0.101	3.53	0.094
fit error	± 0.08	± 0.002	± 0.07	± 0.002	± 0.10	± 0.002	± 0.16	± 0.003
χ^2/d.o.f.	128.8/236		103.7/155		139.6/138		105.9/121	
ren. scale	± 0.03	± 0.004	± 0.08	± 0.003	± 0.21	± 0.003	± 0.21	± 0.001
hadr.	± 0.42	± 0.006	± 0.49	± 0.008	± 0.36	± 0.004	± 0.23	± 0.003
exp.	± 0.07	± 0.003	± 0.31	± 0.005	± 0.23	± 0.003	± 0.67	± 0.009
tot. error	± 0.43	± 0.008	± 0.59	± 0.010	± 0.49	± 0.006	± 0.76	± 0.010

Table 3: Results are shown for fits with the observables $1-T$, C, B_T and B_W to $\alpha_s(M_{Z^0})$ and C_A.

	$1-T$		C		B_T		B_W	
	C_F	$\alpha_s(M_{Z^0})$	C_F	$\alpha_s(M_{Z^0})$	C_F	$\alpha_s(M_{Z^0})$	C_F	$\alpha_s(M_{Z^0})$
fit result	1.11	0.128	1.28	0.114	1.65	0.100	1.98	0.078
fit error	± 0.06	± 0.004	± 0.03	± 0.002	± 0.03	± 0.002	± 0.09	± 0.003
χ^2/d.o.f.	133.4/236		103.6/155		131.3/138		87.8/121	
ren. scale	± 0.05	± 0.004	± 0.05	± 0.003	± 0.01	± 0.003	± 0.07	± 0.001
hadr.	± 0.24	± 0.013	± 0.22	± 0.009	± 0.21	± 0.006	± 0.24	± 0.006
exp.	± 0.10	± 0.008	± 0.04	± 0.001	± 0.17	± 0.008	± 0.27	± 0.008
tot. error	± 0.28	± 0.016	± 0.23	± 0.010	± 0.27	± 0.011	± 0.38	± 0.011

Table 4: Results are shown for fits with the observables $1-T$, C, B_T and B_W to $\alpha_s(M_{Z^0})$ and C_F.

	$1-T$			C		
	C_A	C_F	$\alpha_s(M_{Z^0})$	C_A	C_F	$\alpha_s(M_{Z^0})$
fit result	2.72	1.28	0.124	2.96	1.30	0.114
fit error	±0.13	±0.07	±0.002	±0.18	±0.08	±0.002
χ^2/d.o.f.	127.9/235			103.6/154		
ren. scale	±0.04	±0.00	±0.004	±0.08	±0.00	±0.003
hadr.	±0.10	±0.17	±0.010	±0.12	±0.16	±0.009
exp.	±0.11	±0.13	±0.005	±0.40	±0.10	±0.004
tot. error	±0.20	±0.22	±0.012	±0.46	±0.21	±0.011
	B_T					
	C_A	C_F	$\alpha_s(M_{Z^0})$			
fit result	3.39	1.58	0.097			
fit error	±0.21	±0.06	±0.002			
χ^2/d.o.f.	128.0/137					
ren. scale	±0.10	±0.01	±0.002			
hadr.	±0.16	±0.19	±0.008			
exp.	±0.48	±0.02	±0.005			
tot. error	±0.56	±0.20	±0.010			

Table 5: Results are shown for fits with the observables $1-T$, C and B_T to $\alpha_s(M_{Z^0})$, C_A and C_F.

	$1-T$			C		
	n_f	$\alpha_s(M_{Z^0})$	α_0	n_f	$\alpha_s(M_{Z^0})$	α_0
fit result	6.39	0.121	0.521	4.88	0.111	0.526
fit error	±0.79	±0.003	±0.015	±1.34	±0.004	±0.023
χ^2/d.o.f.	127.9/235			103.4/154		
ren. scale	±0.21	±0.004	±0.001	±0.42	±0.003	±0.005
hadr.	±0.47	±0.001	±0.057	±0.48	±0.001	±0.065
exp.	±0.69	±0.004	±0.010	±2.55	±0.008	±0.038
tot. error	±1.17	±0.006	±0.060	±2.96	±0.010	±0.079
	B_T					
	n_f	$\alpha_s(M_{Z^0})$	α_0			
fit result	3.77	0.108	0.635			
fit error	±1.12	±0.003	±0.019			
χ^2/d.o.f.	132.1/137					
ren. scale	±0.46	±0.004	±0.006			
hadr.	±0.33	±0.001	±0.089			
exp.	±2.97	±0.009	±0.002			
tot. error	±3.22	±0.010	±0.091			

Table 6: Results are shown for fits with the observables $1-T$, C and B_T to $\alpha_s(M_{Z^0})$, α_0 and n_f.

	$1-T$			C		
	C_A	$\alpha_s(M_{Z^0})$	α_0	C_A	$\alpha_s(M_{Z^0})$	α_0
fit result	2.73	0.121	0.528	3.03	0.111	0.525
fit error	$\pm$0.16	$\pm$0.003	$\pm$0.020	$\pm$0.25	$\pm$0.004	$\pm$0.029
χ^2/d.o.f.	128.1/235			103.4/154		
ren. scale	$\pm$0.05	$\pm$0.004	$\pm$0.001	$\pm$0.08	$\pm$0.003	$\pm$0.002
hadr.	$\pm$0.10	$\pm$0.001	$\pm$0.057	$\pm$0.09	$\pm$0.001	$\pm$0.064
exp.	$\pm$0.14	$\pm$0.004	$\pm$0.012	$\pm$0.50	$\pm$0.008	$\pm$0.053
tot. error	$\pm$0.24	$\pm$0.006	$\pm$0.061	$\pm$0.57	$\pm$0.009	$\pm$0.089
	B_T					
	C_A	$\alpha_s(M_{Z^0})$	α_0			
fit result	3.24	0.108	0.626			
fit error	$\pm$0.21	$\pm$0.003	$\pm$0.023			
χ^2/d.o.f.	131.8/137					
ren. scale	$\pm$0.07	$\pm$0.004	$\pm$0.006			
hadr.	$\pm$0.06	$\pm$0.001	$\pm$0.088			
exp.	$\pm$0.60	$\pm$0.009	$\pm$0.086			
tot. error	$\pm$0.64	$\pm$0.010	$\pm$0.126			

Table 7: Results are shown for fits with the observables $1-T$, C and B_T to $\alpha_s(M_{Z^0})$, α_0 and C_A.

	$1-T$			C		
	C_F	$\alpha_s(M_{Z^0})$	α_0	C_F	$\alpha_s(M_{Z^0})$	α_0
fit result	1.42	0.113	0.478	1.49	0.105	0.490
fit error	$\pm$0.21	$\pm$0.009	$\pm$0.041	$\pm$0.31	$\pm$0.011	$\pm$0.074
χ^2/d.o.f.	130.4/235			103.2/154		
ren. scale	$\pm$0.03	$\pm$0.006	$\pm$0.013	$\pm$0.10	$\pm$0.006	$\pm$0.020
hadr.	$\pm$0.03	$\pm$0.001	$\pm$0.053	$\pm$0.06	$\pm$0.002	$\pm$0.059
exp.	$\pm$0.21	$\pm$0.011	$\pm$0.022	$\pm$0.10	$\pm$0.004	$\pm$0.031
tot. error	$\pm$0.30	$\pm$0.015	$\pm$0.072	$\pm$0.35	$\pm$0.014	$\pm$0.103
	B_T			B_W		
	C_F	$\alpha_s(M_{Z^0})$	α_0	C_F	$\alpha_s(M_{Z^0})$	α_0
fit result	2.28	0.085	0.406	3.50	0.052	0.311
fit error	$\pm$0.47	$\pm$0.009	$\pm$0.080	$\pm$0.73	$\pm$0.009	$\pm$0.068
χ^2/d.o.f.	129.4/137			79.1/120		
ren. scale	$\pm$0.88	$\pm$0.029	$\pm$0.222	$\pm$0.44	$\pm$0.005	$\pm$0.031
hadr.	$\pm$0.32	$\pm$0.006	$\pm$0.056	$\pm$0.38	$\pm$0.004	$\pm$0.051
exp.	$\pm$0.80	$\pm$0.018	$\pm$0.248	$\pm$1.44	$\pm$0.023	$\pm$0.284
tot. error	$\pm$1.32	$\pm$0.036	$\pm$0.348	$\pm$1.72	$\pm$0.025	$\pm$0.298

Table 8: Results are shown for fits with the observables $1-T$, C, B_T and B_W to $\alpha_s(M_{Z^0})$, α_0 and C_F.

	$1-T$			
	C_A	C_F	$\alpha_s(M_{Z^0})$	α_0
fit result	2.68	1.21	0.128	0.567
fit error	± 0.19	± 0.26	± 0.016	± 0.093
χ^2/d.o.f.	127.8/234			
ren. scale	± 0.03	± 0.02	± 0.005	± 0.006
hadr.	± 0.16	± 0.14	± 0.010	± 0.042
exp.	± 0.17	± 0.35	± 0.025	± 0.164
tot. error	± 0.30	± 0.46	± 0.032	± 0.194

Table 9: Results are shown for fits with the observables $1-T$ to $\alpha_s(M_{Z^0})$, α_0, C_A and C_F.

fit type		α_0	n_f	C_A	C_F
$\alpha_s(M_{Z^0})$-α_0	α_s	-0.87			
$\alpha_s(M_{Z^0})$-n_f	α_s		0.985		
$\alpha_s(M_{Z^0})$-C_A	α_s			-0.981	
$\alpha_s(M_{Z^0})$-C_F	α_s				-0.997
$\alpha_s(M_{Z^0})$-C_A-C_F	α_s			0.20	-0.68
	C_A				-0.85
$\alpha_s(M_{Z^0})$-α_0-n_f	α_s	0.69	0.97		
	α_0		0.82		
$\alpha_s(M_{Z^0})$-α_0-C_A	α_s	0.78		-0.97	
	α_0			-0.89	
$\alpha_s(M_{Z^0})$-α_0-C_F	α_s	0.96			-0.998
	α_0				-0.975
$\alpha_s(M_{Z^0})$-α_0-C_A-C_F	α_s	0.988		-0.72	-0.985
	α_0			-0.75	-0.970
	C_A				0.59

Table 10: The correlations between the fit parameters for all types of standard fits to the $1-T$ distributions are shown.

	n_f	$\alpha_s(M_{Z^0})$	α_0	C_A	$\alpha_s(M_{Z^0})$	α_0
result	5.64	0.116	0.524	2.88	0.116	0.526
error	± 1.35	± 0.005	± 0.064	± 0.27	± 0.005	± 0.067
	C_F	$\alpha_s(M_{Z^0})$	α_0	C_A	C_F	$\alpha_s(M_{Z^0})$
result	1.45	0.109	0.484	2.84	1.29	0.119
error	± 0.27	± 0.013	± 0.075	± 0.24	± 0.18	± 0.10

Table 11: The combined results based on $1-T$ and C are shown with total errors. The results for C_A, C_F and $\alpha_s(M_{Z^0})$ are from fits with α_0 fixed.

Figures

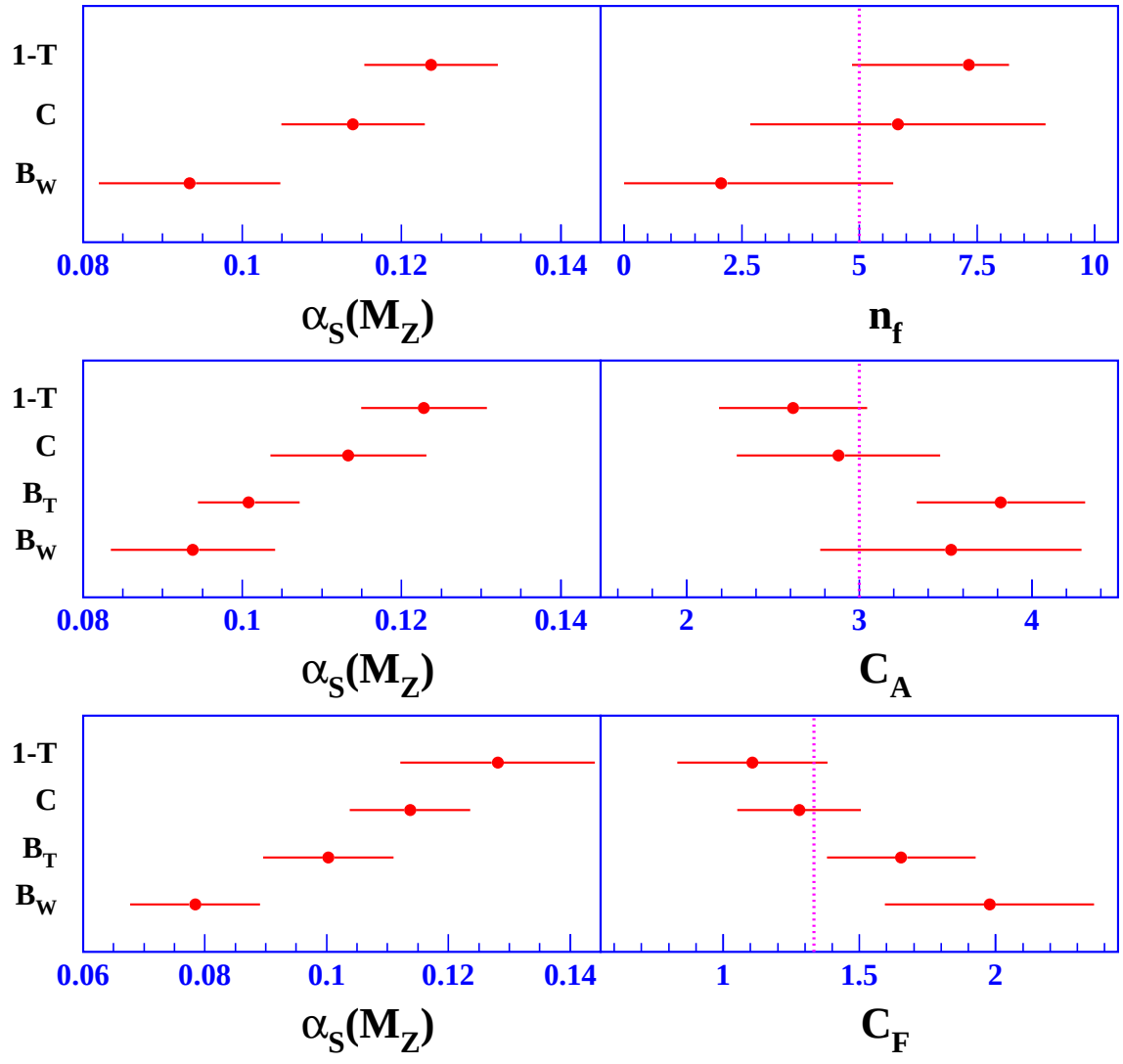

Figure 1: The figures present results of fits to $\alpha_s(M_{Z^0})$ and one of the colour factors n_f, C_A or C_F with observables as given on the vertical axis. The vertical dotted lines indicate the expectation from standard QCD for the colour factor.

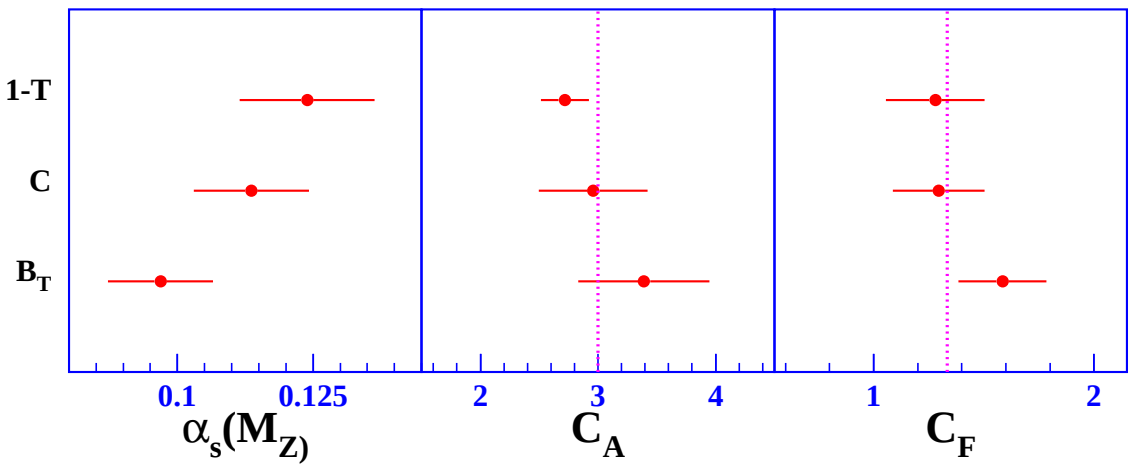

Figure 2: The figure presents results from fits to $\alpha_s(M_{Z^0})$ and the colour factors C_A and C_F with observables as given on the vertical axis. The error bars show total uncertainties. The vertical dotted lines indicate the expectations from standard QCD for the colour factors.

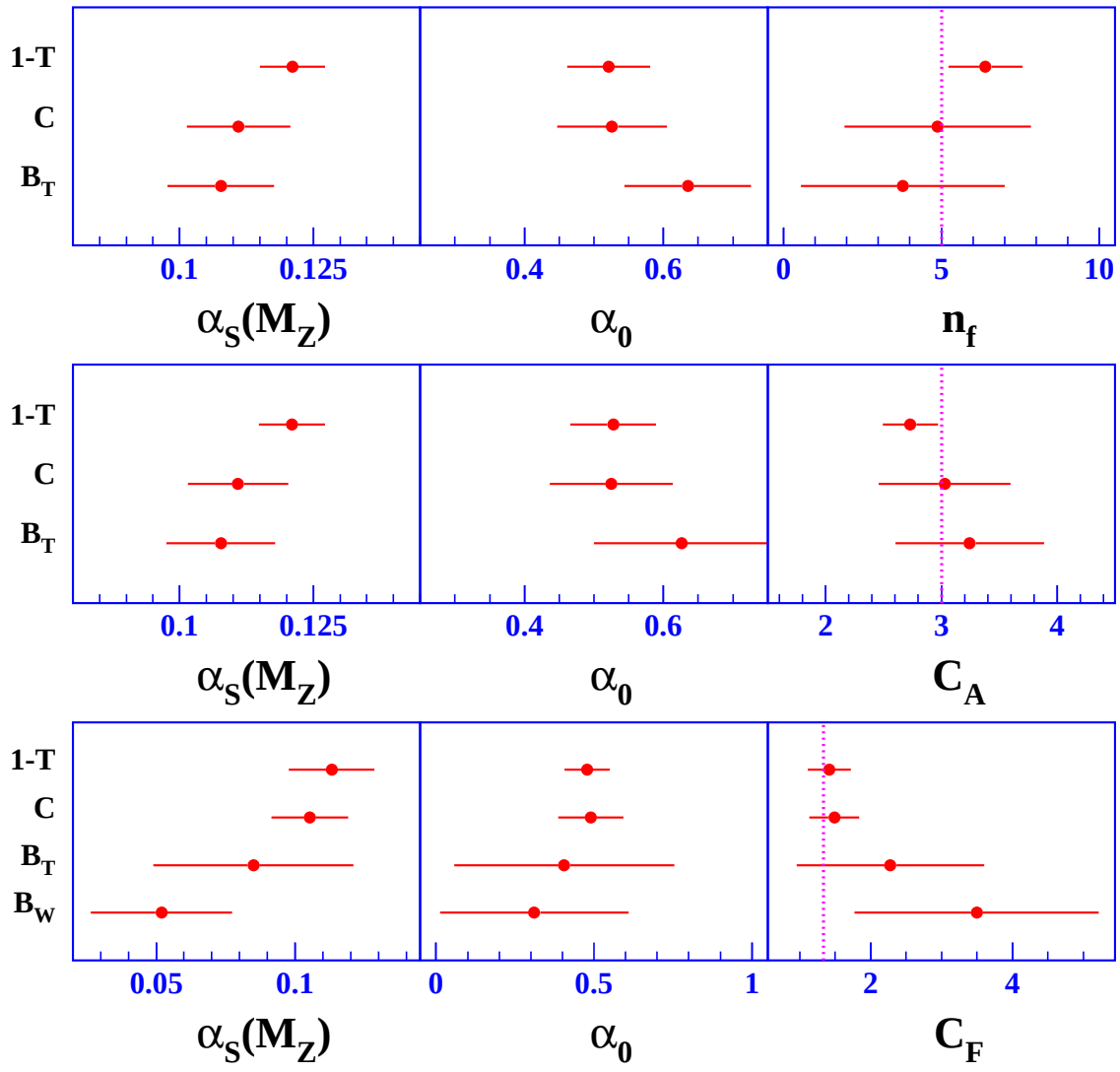

Figure 3: The figures present results from fits to $\alpha_s(M_{Z^0})$, α_0 and one of the colour factors n_f, C_A or C_F with observables as given on the vertical axis. The error bars show total uncertainties. The vertical dotted lines indicate the expectation from standard QCD for the colour factor.

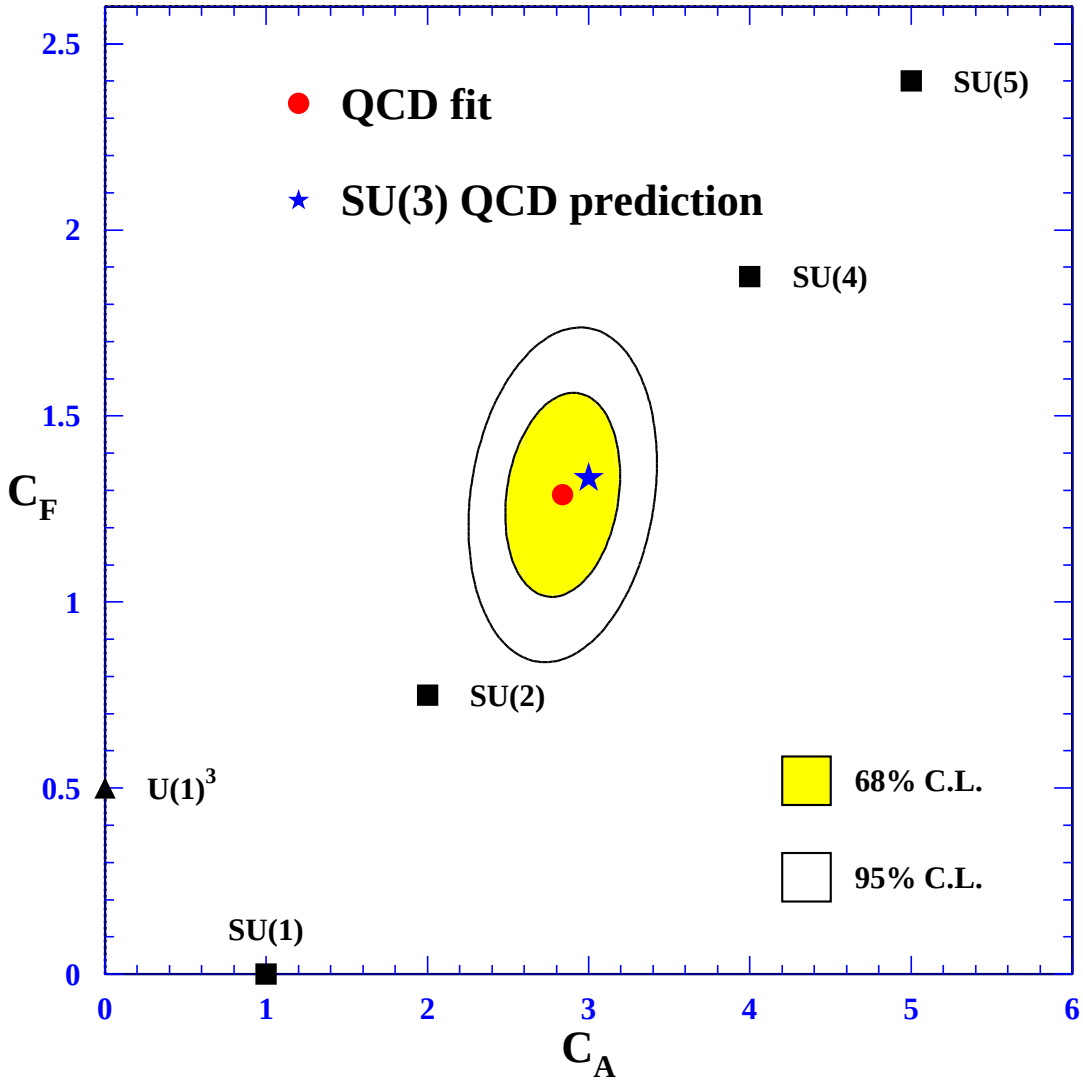

Figure 4: The figure presents the combined results for the colour factors C_A and C_F from fits to $\alpha_s(M_{Z^0})$, C_A and C_F based on the observables $1-T$ and C. The square and triangle symbols indicate the expectations for C_A and C_F for different symmetry groups.